INSTITUTE FOR DIRECT ENERGY CONVERSION

TOWNE SCHOOL

UNIVERSITY OF PENNSYLVANIA

PHILADELPHIA, PENNSYLVANIA

STATUS REPORT

INDEC-SR-6

NATIONAL AERONAUTICS AND SPACE ADMINISTRATION

GRANT NSG-316

July 1, 1965

INSTITUTE FOR DIRECT ENERGY CONVERSION

TOWNE SCHOOL

UNIVERSITY OF PENNSYLVANIA

PHILADELPHIA, PENNSYLVANIA

STATUS REPORT

INDEC-SR-6

NATIONAL AERONAUTICS AND SPACE ADMINISTRATION

GRANT NSG - 316

July 1, 1965

TABLE OF CONTENTS

LIST OF ILLUSTRATIONS

1. MATERIALS ENGINEERING

Acting Branch Chief: Dr. Leonard Nanis

Senior Members: Dr. Geoffrey Belton, Dr. Ram A. Sharma

1. 1 Transient Measurement of Thermal Diffusivity of Refractory Materials at High Temperature

Dr. Manfred Altman; H. Chang

The average thermal conductivity of LiF was reported by McKinnon, (1) Vild and Milko to be 5.1 BTU/hr. ft. ^{o}F with a maximum potential error of 19.5 per cent. Using a density of 162.56 lb/ft^{3} (2) and specific heat of 0.373 BTU/lb.^{o}F for LiF, the thermal diffusivity, α, was calculated to be 3.3 x 10^{-3} in^{2}/sec. The method used by McKinnon, et al. was of the steady state type. A module 10"x10"x3" contained the lithium fluoride and was constructed with top and bottom plates of 1/4" Haynes 25 plate and sides of .063" Haynes 25 sheet material. The module was heated from above with six 1000 watt capacity infrared quartz heaters. Heat was removed from the bottom of the module by air flowing through a square rectangular box. The heat removal rate of the air was used to determine the heat transfer. To this value was added 1/2 of the module side heat loss obtained from previous steady-state calibration tests. Error in the net heat input was due to the losses which are difficult to determine accurately.

In the present study LiF was chosen as the material to be tested first for the following reasons:

1. LiF has a low melting temperature, 848^{o}C, so that it is possible to prepare the polycrystalline samples readily in a high frequency furnace.

2. Diffusivity data from Ref. 1 may be used as a reference for comparison with LiF data obtained by the present unsteady state method.[3]

N65-35126

Cylindrical samples of LiF were generated by melting LiF powder (Fisher Certified Reagent powder) in a carbon crucible. The samples are 6" long and 1" diameter. The carbon crucible served both as the melt container and the susceptor for the high frequency induction furnace. These cylinders are at present being drilled to accommodate a 1/8" hole in the center, 3" deep from the bottom end of the sample. A pair of thermocouples made out of .016" chromel-alumel wires will be inserted into this hole through high purity alumina insulators with the bead touching the end of this hole. An identical thermocouple from the same lot of wires will be attached to the surface of the sample 3" from the bottom of the sample. The bead of this surface thermocouple will be inserted into a samll indenture on the surface of the sample and then tied to the sample by a piece of platinum wire. An alternate drilling procedure is being tried to obtain two 1/16" holes 2 3/4" deep from the bottom end of the sample. One of the holes is at the center of the sample and the other is close to the wall and centered 0.45" from the center hole. Two thermocouples made out of 0.010" platinel wires may be inserted into the holes through high purity alumina and with the bead touching the end of the holes. The fragility of the LiF samples requires extreme care in drilling, especially for holes close to and parallel with the surface. This apparatus for the unsteady state method consists of a platinum-40% rhodium wire-wound furnace which gives temperatures up to 1750^{o}C, a programmed controller with

silicon-controlled rectifier to raise the temperature of the furnace, an adjustable zero and adjustable range recorder for recording the temperature, and a recorder with a 10 mv range for recording the differential E.M.F which is amplified by a D.C. amplifier before being fed to the recorder.

The desired uniform heating rate of the furnace is obtained by means of a motor-driven cam which drives the control point of the proportional controller and so varies D.C. voltage. This D.C. voltage is applied to a silicon-controlled rectifier which regulates the power to the furnace windings.

By this arrangement, it is possible to raise the temperature of the furnace at a uniform rate from 3 to 20 centigrade degrees per minute. Lower heating and cooling rates have been achieved by lowering the rotation speed of the cam by including an adjustable interrupter in the power supply to the motor. The adjustable zero and adjustable range recorder are internally standardized.

An alumina reaction tube 1.5" in diameter and 42" long is supported in the furnace winding tube. To the top end of the reaction tube was attached a silicone rubber stopper with an alumina rod through the center. A platinel thermocouple was inserted in this rod half way down the furnace. The output of this thermocouple was fed directly to the programmed controller. It is found in the present modification however

that the heat input to the furnace can be simply controlled manually to obtain the constant rate of rise of temperature on the surface of the sample. The temperature of the sample on the surface was recorded on the adjustable zero and adjustable range recorder. The furnace system has been thoroughly tested and measurements await the production of a suitable LiF sample.

The two thermocouples in the sample, one at the center and the other close to the surface, will be connected differentially so that the difference of those temperatures is recorded on the 10 mv range recorder.

In these tests the thermal diffusivity is calculated by using the formula

$$\alpha = \frac{a^2 k}{4\theta}$$

where a - Distance between the two thermocouples,/inches

α - Thermal diffusivity in $in^2/sec.$

k - Rate of rise of surface temperature, $^{\circ}C/sec.$

θ - Temperature difference between two thermocouples $/^{\circ}C.$

The errors involved in their measurement can be evaluated from the expression

$$\frac{\partial \alpha}{\alpha} = \frac{\partial k}{k} + \frac{\partial \theta}{\theta}$$

k can be read accurately within $\pm$ 2.5% (1 mv was measured to within an accuracy of $\pm$ 0.025 mv). θ is read accurately with $\pm$ 1.25% (200 microvolts accurate to within 2.5 microvolts). The maximum error introduced in the computation of α would be $\pm$ 3.75%. The value of k was held to an accuracy of 2 - 3% during a test run. The minimum experimental reading error introduced in the value of τ is estimated to be $\pm$ 6.75%

The following instruments are being used in the experiment, with associated accuracies:

Instruments	Rated Accuracy
Leeds & Northrup Speedomax H	$\pm$ 0.5%
Leeds & Northrup Speedomax H Centre-Zero Recorder	$\pm$ 0.5%
Leeds & Northrup Stabilized D-C Microvolts Amplifier	$\pm$ 2%

Thus, the instrumentation used introduces a maximum error of $\pm$ 3%. Thermal conductivity values as a function of temperature will be obtained and presented in the next report.

References:

1. R. A. McKinnon, T. J. Vild and J. A. Milko "Design Study of Solar Brayton Cycle Cavity Receivers with Lithium Fluoride Heat Storage" AIAA Paper No. 64-727.

2. "Handbook of Chemistry and Physics", 44th Ed. The Chemical Rubber Publishing Co.

3. Han Chang "An Unsteady - State Method for Measuring Thermal Diffusivity of Eutectic Mixtures of Refractory Materials at High Temperatures", unpublished.

1.2 Partial Molar Properties of Magnesium Base Binary Thermal Energy Storage Systems

Dr. Geoffrey Belton; Y. Rao

In recent years intermetallic compounds have been favorably considered as potential thermal energy storage materials.[1] The factors that are generally considered in selecting a suitable thermal energy storage material are:

1) Heat of fusion in calories /gram - not less than 200 cals /gram.
2) Melting point - above 900°C.
3) Ease with which it can be contained in liquid state.
4) Chemical stability and vaporization characteristics.

Materials such as Mg_2Si and Mg_2Ge melt at $1100 \pm 10^{\circ}C$ and have relatively large heats of fusion. The problem of finding a suitable container can be solved if the reactions that might occur between the container and these thermal energy storage materials are studied. Free energy data for the systems Mg-Si and Mg-Ge would not only determine the criteria of equilibrium in such reactions but also help in estimating the activity and vaporization characteristics of magnesium. Experimental work was started with a view of obtaining these data.

Of the various methods available for the purpose, the establishment of

a galvanic cell, the emf of which is a measure of the free energies concerned, is by far the most advantageous. A description of the apparatus and the technique was given in a previous report.[2]

Preparation of the Materials:

Pure magnesium was obtained from Fisher Scientific Co. and fulfils ASTM specifications. Pure silicon (99.9%) was supplied bythe Sargent & Co., New Jersey. A free sample of high purity Ge was generously furnished by the Bell Laboratories, Murray Hill, N.J.

Magnesium metal boils at 1105°C and 1 atmosphere [3] while magnesium disilicide and silicon melt at 1100°C[4] and 1418° C[4] respectively. Under these conditions the best method of preparing Mg_2Si was found to consist of facilitating the liquid (Mg) - solid (Si) interaction over a long period of time at temperatures suitably below the boiling point of Mg, e.g. 950°C. This prolonged heating was followed by a final increase to 1100°C. Weighed quantities of Mg and Si were taken in a graphite vessel. About 1% of the total weight of Si was added to compensate for its loss as SiC[5]. Quantitative analysis of the final product yielded a Mg content of 66.15 atom percent.

Preparation of Mg_2Ge is much easier because Ge melts at 936°C, thus permitting liquid (Mg) - liquid (Ge) interaction to take place at a much faster rate. Weighed quantities of magnesium and germanium were mixed in an alumina crucible and slowly heated to 950°C. Violent reaction accompanied the formation of Mg_2Ge. After the reaction subsided, the

crucible temperature was raised to about 1150^{o} and followed by a slow cooling. The magnesium content was found to be 66.1 atom percent

Electrolyte:

Dry magnesium chloride (30% mol.) and calcium chloride (70% mol.) mixture was prepared from the previous stock of dehydrated salts.[2]

Temperature Control & Measurement:

The furnace consists of 2"x30" alumina tube on which 0.020" dia. Pt.10% Rh wire was wound. It is equipped with a Barber Colman Co. Capacitrol and a silicon controlled rectifier to maintain a constant temperature. The furnace has a uniform temperature zone of about 3" in the the center. In steady state, the temperature variation in the cell did not exceed 0.3^{o}C over a period of 12 hours.

Cell E.M.F. Measurements:

A Leeds and Northrup portable potentiometer was used to measure the cell emf s. The cell was maintained at a given temperature for at least 2 hours for the attainment of equilibrium. Emf readings were taken every half hour. For values as high as 200 mV, only a variation of $\pm$ 0.05% was tolerated. To test the reversibility of the cell, after a reading was taken an opposing emf was applied and the subsequent readings were compared with the earlier ones. Both sets must be equal for a cell that has attained equilibrium.

Results:

The experimental emf vs T data for Mg_2Si and Mg_2Ge (both vs a pure magnesium electrode) are shown in Figures 1.2 -1 and 1. 2-2 respectively.

The linear dependence of emf upon temperature shows that the entropy is independent of temperature. The galvanic cells may be represented as

I. $Mg(1) \,/\, (Mg^{++}) \,/\, Mg_2Si(S) + Si(S)$

II. $Mg(1) \,/\, (Mg^{++}) \,/\, Mg_2Ge(S) + Ge$ (S or 1)

Emf vs T data permit the calculation of the thermodynamic properties of the reactions:

$$2\ Mg\ (1) + Si(S) = Mg_2Si(S)$$

$$2\ Mg\ (1) + Ge(1) = Mg_2Ge(S)$$

The free energy change, ΔF, of the cell reaction at any given temperature is related to the reversible electromotive force, E, by

$$\Delta F = - NFE$$

In the above reactions all substances involved are in their standard states (activity equal to unityj) and the free energy change becomes the standard free energy of formation ΔF^{O}. The heat of formation, ΔH^{O} is calculated from the ΔF^{O} and the temperature coefficient of the electromotive force. The results were summarized in Tables 1. 2-1 and 1. 2-2.

Investigation of the Thermodynamic Properties of the Electrolyte:

The electrolyte used was a mixture of $CaCl_2$ and $MgCl_2$. Mixtures have been preferred to pure salts because of their lower melting points and less vaporization at high temperatures. In this work, electrolytes of varying $MgCl_2$ contents (8% mol - 50% mol) have been used. In order to determine the free energies of mixing over the entire composition range of the system $MgCl_2$ - $CaCl_2$, a chlorine electrode was used in conjunction with a Mg - electrode. The formation cell is

$$Mg\ (1) \Big/ MgCl_2 - CaCl_2\ (1) \Big/ Cl_2(g),\ C$$

and the reaction is

$$Mg\ (1) + Cl_2\ (g) = (MgCl_2)\ (1)\ \text{mixture}$$

The emf of the cell was measured at various temperatures for a given composition of the electrolyte. The data are summarized in (Fig. 1.2-3). The activity of $MgCl_2$ can be deduced from

$$E_1 = E^o - \frac{RT}{NF} \ln a_1$$

E_1 = emf of the cell

E^o = emf for pure $MgCl_2$

a_1 = activity of $MgCl_2$

Mg-Al alloys were studied using this electrolyte and the thermodynamic data are summarized in Table 1.2-3.

Discussion:

Intermetallic compounds such as Mg_2Si, Mg_2Ge, Mg_2Pb and Mg_2Sn are transition cases approaching typical salt-like bonding; as a rough approximation one may write $(Mg^{2+})_2\ Si^{4-}$ etc. The formation of intermetallic compounds with ordered structures appears to be a direct consequence of the existence of charged species with opposite signs.

Both Mg_2Si and Mg_2Ge have CaF_2 (C_1 type) structure. The lattice constants, melting points and heats of formation for these and also for the compounds Mg_2Pb and Mg_2Sn are listed in Table 1.2-4.[7,8,9] It is interesting to notice that the higher the heat of formation, the higher is the melting point of the compound.

References:

1. Status Report, INDEC-SR-5, Jan. 4, 1965, p.2-2.

2. Status Report, INDEC-SR-4, June, 1964, p.22.

3. K. K. Kelley, Bulletin U.S. Bureau of Mines, 1935, No. 383, Critical Evaluation of Vapour Pressures and Heats of Evaporation of Inorganic Substances.

4. O. Kubaschewski and E. U. Evans, Metallurgical Thermochemistry, p. 297, Pergamon Press (1958)

5. Preparation of Mg_2Si and Mg_2Ge, R. Labetz, M. Donald, J. Electrochem. Soc. 110, p.121 (1963)

6. O. Kubaschewski and H. Villa,Z. Elektrochem (1949)53,p.32.

7. W. Klemm and H. Westlinning, Z. Anorg. Chem. 245, 1940, p.365-380.

8. Wagner, C. and G. Engelhardt, Z. Physik. Chem.Vol. 159, 1932, p. 241-267,Study of Mg - Pb alloys by electromotive force method.

9. "Thermodynamics Data of Alloys", O. Kubaschewski & J. A. Catterall, Pergamon Press (1956)

TABLE 1.2-1

Electromotive Force Data for
2 Mg(1) + Si (S) = Mg_2Si(S)

Temp.°C	E.M.F.(mv)
731.7	130.48
792.6	125.79
826.7	122.28
849.7	121.0
861.5	119.0
876.2	118.20
889.4	117.40
908.7	115.62
935.62	113.45
963.9	109.80
980.3	106.3
997.5	101.23
1004.0	99.12
1026.7	92.87

TABLE 1.2-2

Electromotive Force Data for
2 Mg(1) + Ge (1) = Mg_2Ge (S)

Temp.°C	E.M.F.(mv)
697.5	220.60
714.5	216.40
745.6	208.50
758.3	205.10
797.6	194.80
831.8	185.20
852.4	178.80
880.0	170.9
918.6	158.62
951.1	147.8
984.7	135.20
1007.2	126.00
1020.0	121.10
1038.4	113.70

TABLE 1.2-3 - Experimental Data for Liquid Mg - Al system at 800°C

Alloy No.	X_{Mg}	E(mv)	$\left(\frac{\partial E}{\partial T}\right)$ mv/100°C	a_{Mg}	γ_{Mg}	F,H in Calories Per gram Molecule S in e.u.*					
						$-F^M_{Mg}$	$+S^M_{Mg}$	$-H^M_{Mg}$	$-F^M$	S^M	$-H^M$
1 - 1	0.096	168.62	9.450	0.02601	0.271	7780	4.360	3102	938.7	0.5116	389.8
1 - 2	0.140	137.36	7.900	0.05116	0.3655	6338	3.645	2427	1276.0	0.6849	541.0
1 - 3	0.2089	106.63	5.618	0.0995	0.4762	4920	2.592	2139	1615.3	0.8831	667.8
2 - 1	0.2451	90.92	4.924	0.1432	0.5843	4195	2.272	1757	1775.1	0.9738	730.0
2 - 2	0.3400	69.94	4.155	0.2215	0.6513	3227	1.917	1170	2000.1	1.0990	820.6
1 - 4	0.4211	52.10	2.834	0.3222	0.7652	2404	1.298	1012	2091.1	1.1595	846.1
1 - 5	0.5166	36.26	2.180	0.4562	0.8833	1673	1.006	594	2072.7	1.1691	817.7
2 - 3	0.6680	19.27	1.426	0.6591	0.9865	889.0	0.658	183	1804.3	1.0608	666.3
2 - 4	0.7000	17.68	1.296	0.6821	0.9743	816.0	0.598	174	1713.1	1.0185	621.1
2 - 5	0.7992	10.57	.88	0.7956	0.9954	487.6	0.4059	52.1	1350.3	0.8440	444.8
1 - 6	0.8440	7.77	.67	0.8453	1.002	358.4	0.3091	26.7	1141.6	0.7278	360.7
1 - 7	0.9192	3.85	.36	0.4200	1.001	177.7	0.1665	-1.0	709.2	0.4827	191.4

*e.u. = cal/gm.mol./deg.C

TABLE 1.2-4

Compound	Lattice Constant	M.P. ^{o}C	Heat of Formation at $1000^{o}K$
Mg_2Si	6.338 ± 0.002 Å	$1085 \pm 15^{o}C$	- 18,000 cals/mol.
Mg_2Ge	6.380 ± 0.002 Å	$1115 \pm 5^{o}C$	- 40,000 cals/mol.
Mg_2Sn	6.762 ± 0.002 Å	$778^{o}C$	- 3,300 cals/mol.
Mg_2Pb	6.799 ± 0.002 Å	$550^{o}C$	- 1,930 cals/mol.

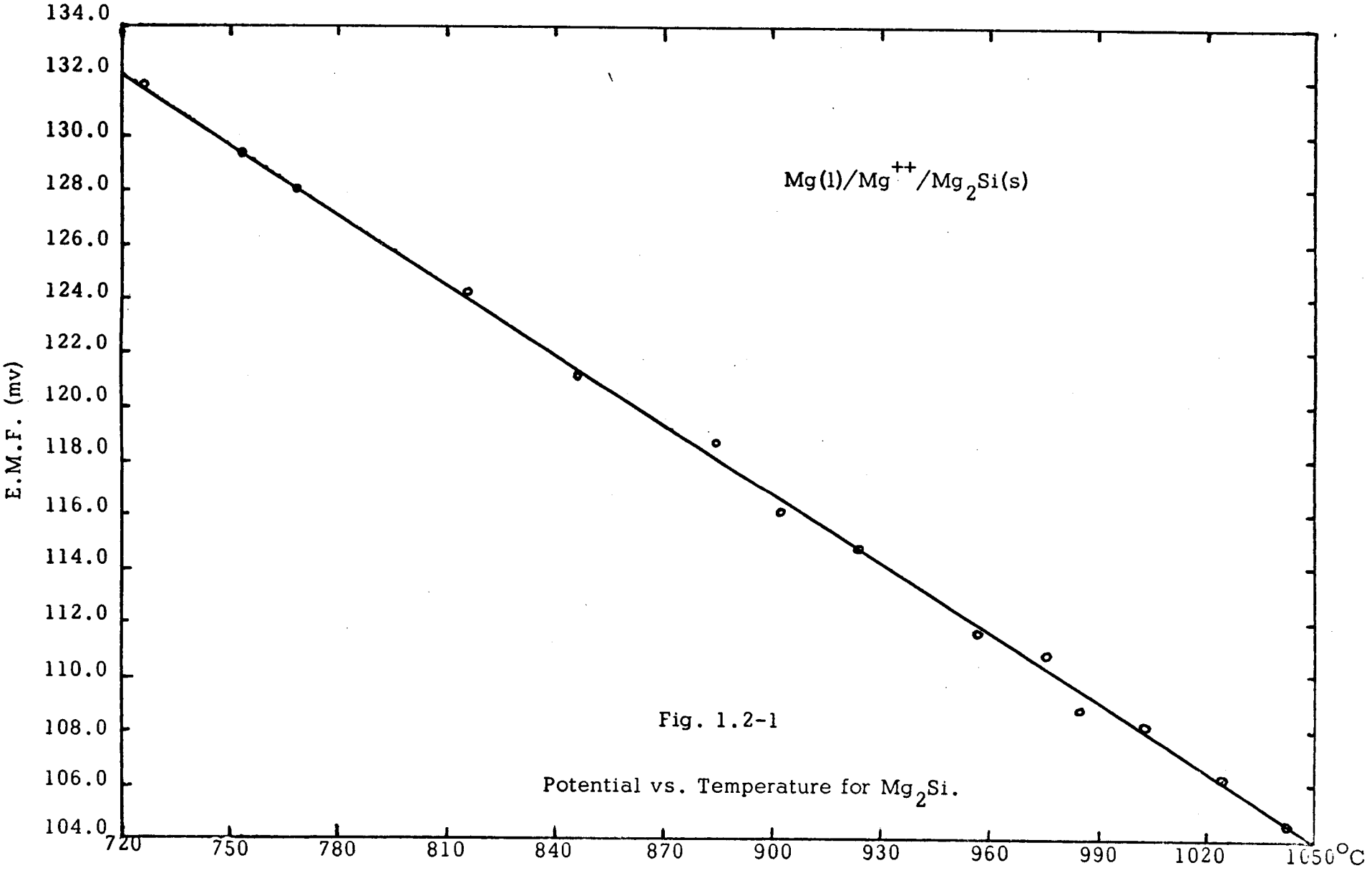

Fig. 1.2-1

Potential vs. Temperature for Mg_2Si.

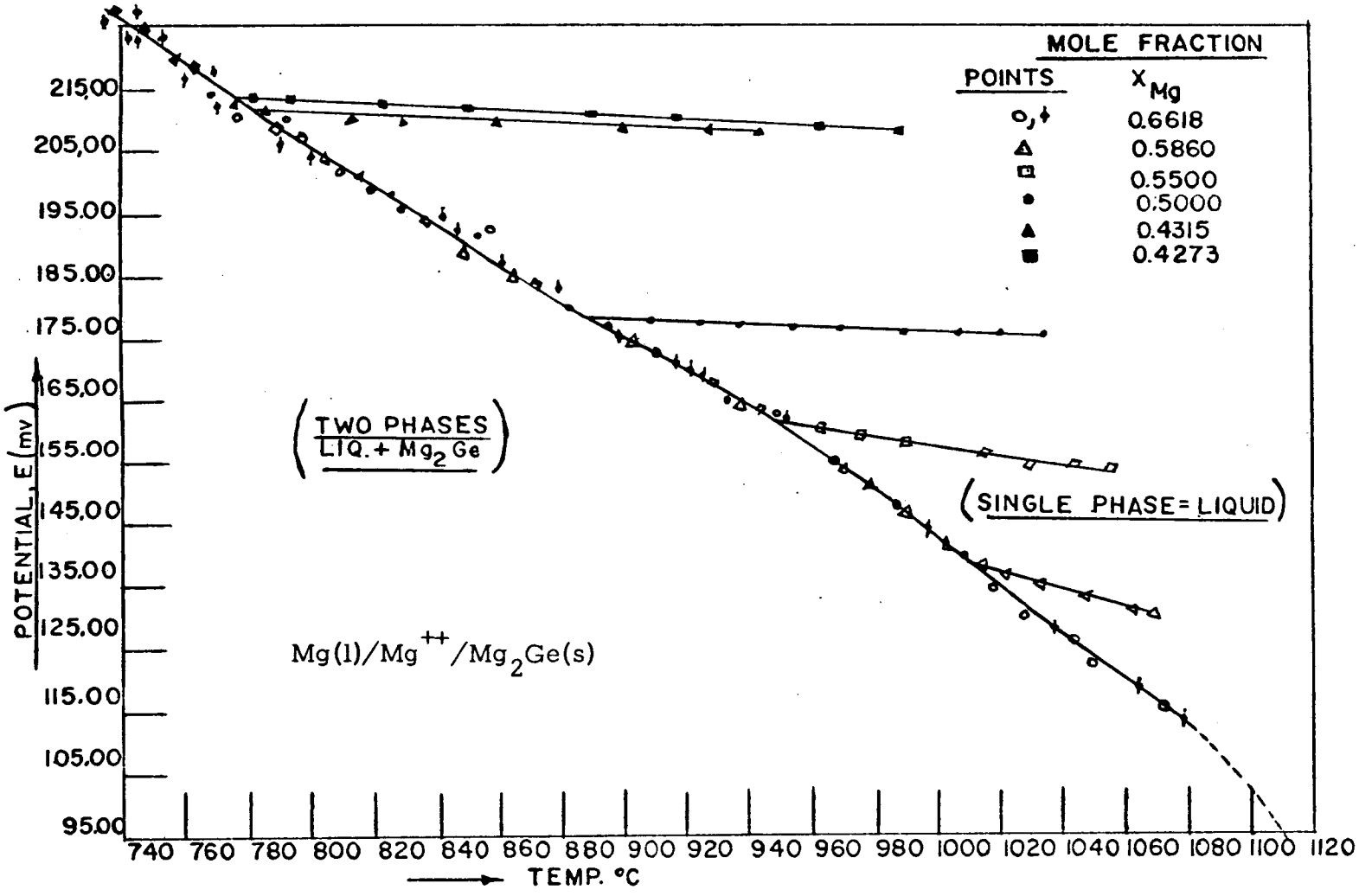

Fig. 1.2-2

Potential vs. Temperature for Mg_2Ge.

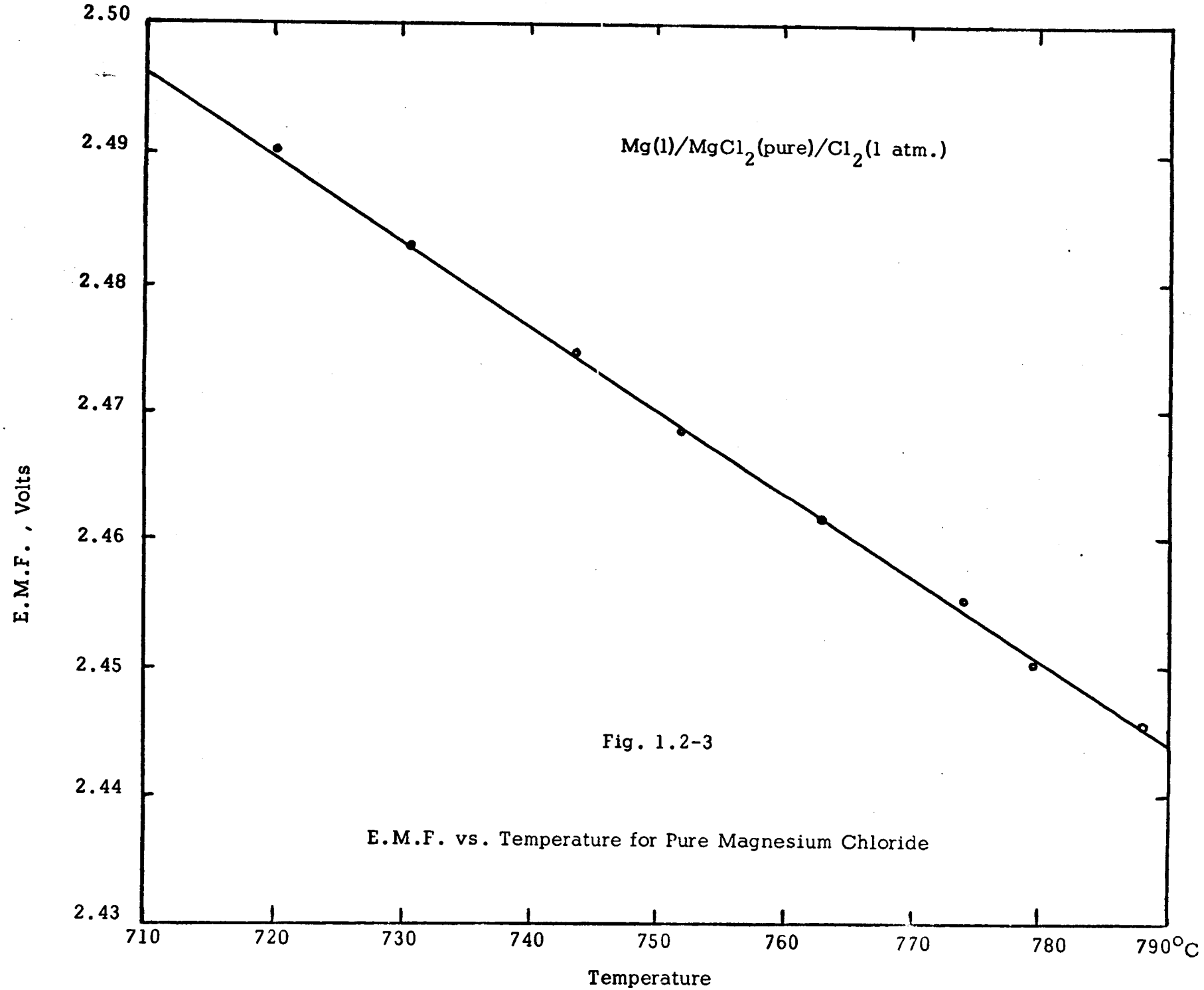

Fig. 1.2-3

E.M.F. vs. Temperature for Pure Magnesium Chloride

1.3 Volume Change on Fusion for Chlorides and Fluorides

Dr. Ram A. Sharma

Introduction:

Most ionic materials increase in volume on melting. The knowledge of this increase is helpful in elucidation of the melting processes.[1,2,3,4] Some of the materials under investigation are intended to be used for thermal energy storage. Volume change measurements are essential for design purposes. The data reported in the literature are sparse and show poor agreement. They have been obtained by the techniques which involve measurements of the density of a sample in solid and liquid states. The density in the liquid state is usually measured by the Archimedes method. A bob of precious metal is used for buoyancy weighings in the case of corrosive liquids.

Density in the solid state near the melting point is much harder to evaluate because the dilatometric methods for polycrystalline materials are often inapplicable at high temperatures due to the unavailability of a suitable inert confining fluid. X-ray measurements of lattice expansions at these temperatures are not suitable as they cannot measure volume changes due to lattice defects appearing in a solid approaching melting point. Measurements of linear expansions of single crystals which generally involve the application of a small mechanical pressure are unsatisfactory as plastic deformation occurs near these temperatures.

Two methods which have been reported for measuring the volume changes of chlorides and fluorides are crystallisation pyknometry[5] and high temperature gas densitometry.[6] In crystallisation pyknometry, the density of a sample in the solid state has been determined at its melting point by trapping the liquid under investigation in a specially designed pyknometer and solidifying it there. By combining these data with those for the liquid, the volume change on fusion may be determined. The major difficulty in this method is the void space created by the dissolved gases in the materials under investigation on solidification and so the solid volume is always apparently greater than actual. The volume change on melting, measured by this method will also include the error involved in the measurement of liquid volume by the Archimedes method.

In high temperature gas densitometry, salt expansion in the solid state is measured by a high temperature gas densitometer from room temperature to just below the melting point. As the solid densities at room temperature and liquid densities over a range of temperatures near to melting point are generally available, the molar volume change on fusion may be obtained by combination of the above measurements. The method suffers from the disadvantage that the gas used in the system may be absorbed progressively with the rise of temperature. Also, lattice defects which develop generally near the melting point may contribute towards more gas absorption.

In the present investigation use was made of a very simple technique in which volume change on fusion has been obtained by measuring the volume of the cavity formed at the top of the sample during solidification and the volume of the solid so obtained. If V_f is the volume of the cavity and V_s the volume of the solid, then the percentage volume change on fusion is given by $\frac{\Delta V_f}{V_s} \times 100$. The volume of the cavity is obtained from the weight of the mercury required to fill the cavity. The volume of the solid is also measured from the weight of mercury displaced by the solid. Densities of the samples have also been calculated from the weights of the samples and the volumes as a check on the possibility of void formation in the sample on solidification.

As seen in (Fig. 1) a high frequency furnace has been used for heating. The sample holder, made of either platinum or graphite, is enclosed in a glass tube. The sample holder is supported on an alumina block with two holes, one in the center and another near the periphery. The peripheral hole is used to introduce argon for maintaining an inert atmosphere. The central hole is used for measuring the temperature by means of an optical pyrometer and also to strike an argon jet at the base of the container to initiate the nucleation for solidification of the salt during the cooling cycle. The sample holder is slowly heated to a temperature slightly above the melting point of the salt. It is kept at this temperature until the dissolved gases are removed. It is then slowly

cooled to the salt melting temperature and the argon jet is directed at base of the holder to initiate solidification and the whole sample is then solidified by reducing the power of the furnace and slowly sliding down the entire fixture from the high frequency furnace coil. By allowing the sample to solidify in this way, a cavity at the top is formed. Experiments have been conducted to measure the volume changes on fusion for LiCl, NaCl, KCl, $CaCl_2$, LiF, KF, MgF_2, BaF_2, $BaCl_2$. All the samples used were of chemical grade. The results together with those available in the literature are given in Table 1.3-1

The validity of the volume change on melting by the cavity method depends upon the assumptions that 1) the temperature of the melt was uniform above and at the melting point when solidification commenced at the walls of the container and 2) the contraction of the cavity was proportional to the contraction of the solid from the melting point to room temperature. In view of the small size of the sample and the relatively high thermal conductivity of the container, the temperature can be maintained uniform within reasonable limits while the second assumption is quite reasonable in view of the cavity being surrounded by the material. Each value reported in Table 1.3-1 is a mean of at least 4 measurements so that the order of magnitude of $\frac{\Delta V_f}{V_s}$ may be regarded as reasonably well established within the range of uncertainity assigned. Although the pyknometric and gas densitometric methods have utility, the present

method is generally applicable, especially at extremely high temperatures (ca. 2000°C).

The values of $\frac{\Delta V_f}{V_s}$ for NaCl and KCl, and LiF as seen in Table 1.3-1 are in good agreement with those reported in the literature, while the rest of the materials are in poor agreement. The values of $\frac{\Delta V_f}{V_s}$ are between 5% and 30% which are quite reasonable as they are expected on the basis of lattice deformation and formation of the holes in these ionic melts.[4] The theories proposed in the literature are as yet unable to give a satisfactory quantitative interpretation of the volume changes obtained for these ionic melts.

References:

1. Al Maholi and Ubbelohde, Proc. Roy. Soc. A 1953, 220, 143.

2. Rogers and Ubbelohde, Trans. Faraday Soc. 1950, 46, 1051.

3. Johnson, Agron and Bredig, J. Am. Chem. Soc. 1955, 77, 2734.

4. Bockris, J. O'M., and Richards, N.E. Proc. Roy. Soc. 1957, 44,241.

5. Landon, G.J. and Ubbelohde, A.R., Trans.Faraday Soc. 1956,64,647.

6. Bockris, J.O'M., et al, J. Phys. Chem. 1960, 64, 507.

7. Bockris, J.O'M., et al Re vue de Chimie, 1962, 7, 60.

8. Shinke, H., et al, Z. anorg. allgem. Chem. 1956, 287, 313.

Table 1.3-1

Materials	Volume Change on Melting			Densities gm/cc
	Present Work	Literature	Reference	
LiCl	34.9 ± 2%	26.2	8	1.91 ± .02
NaCl	24.8 ± 1.2%	25.58,25.0	7,8	2.02 ± .03
KCl	19.02 ± 1.2%	20.20,17.3	7,8	
$CaCl_2$	7.5 ± 1%	0.09	7	2.3 ± .03
$BaCl_2$	12.6 ± 1.4%	3.5	8	3.5 ± 0.06
LiF	28.8 ± 1.5%	29.4	8	2.56 ± 0.03
NaF	19.5 ± 1.5%	27.4	8	2.65 ± 0.04
KF	23 ± 1.2	17.2	8	2.40 ± .05
MgF_2	14.5 ± 1.2%	-		3.06 ± 0.1

CONTROLLED SOLIDIFICATION APPARATUS

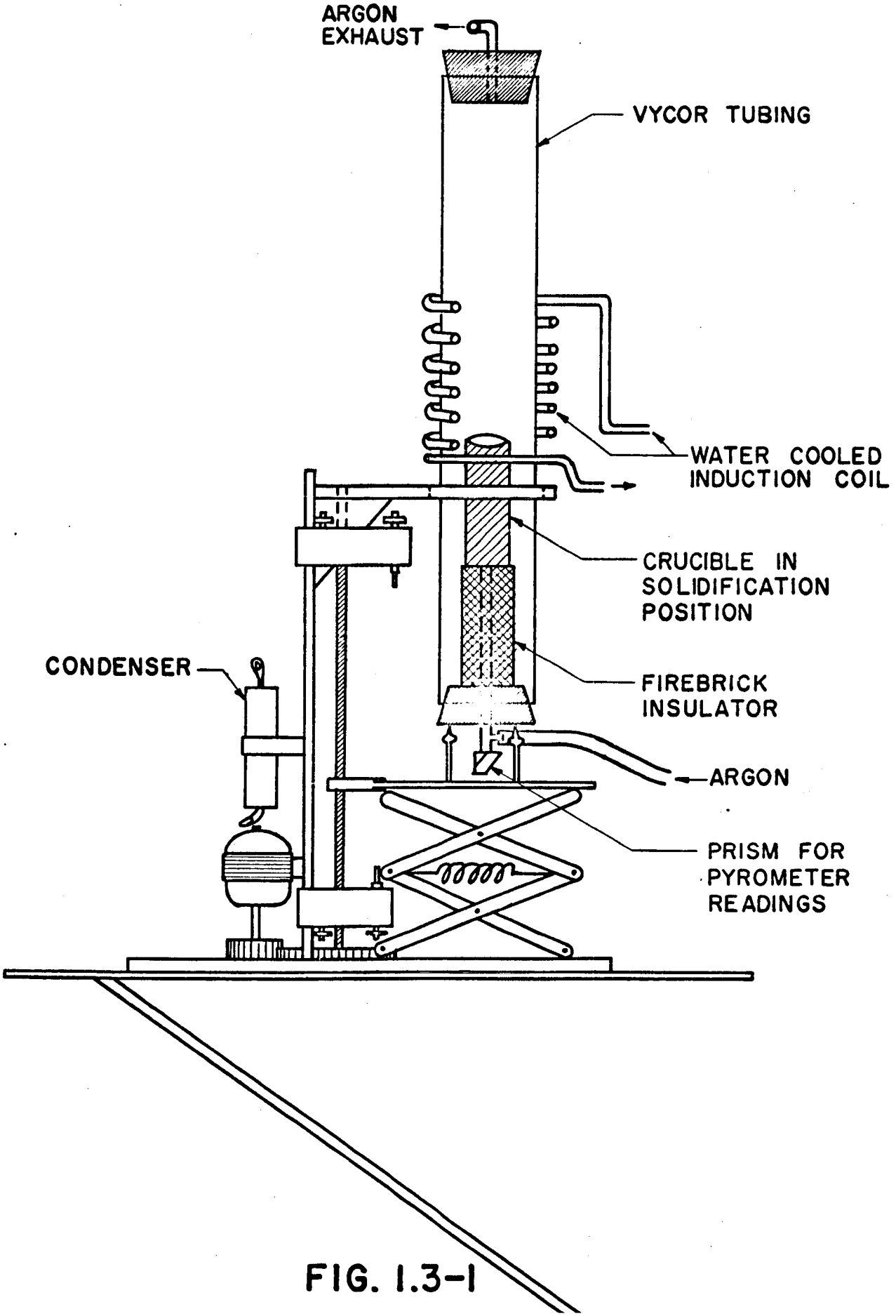

FIG. 1.3-1

2. PLASMA ENGINEERING

Branch Chief: Dr. George L. Schrenk

Senior Members: Dr. Hsuan Yeh, Dr. Leon W. Zelby,

Dr. Chad F. Gottschlich

2.1 Investigation of Na-K Seeded Argon Plasma

Dr. Hsuan Yeh, Dr. Chad F. Gottschlich; T. K. Chu

The research reported here is a continuation of efforts discussed in previous progress reports. The objective of this work is to measure non-equilibrium ionization and its effects in an alkali metal (Na-K) seeded argon plasma, where the non-equilibrium ionization is produced by an externally applied electric field. Measurements of the electric field, plasma current, and spectrophotometric measurements of the radiation from the plasma will be made. These spectrophotometric measurements are especially significant because, by proper interpretation, the radiation yields information on the local properties of the plasma -- e.g., the electron and atom-ion spatial temperature distributions, etc. From these spectrophotometric measurements, electrical measurements, and separate measurements of the pressure and chemical composition of the plasma, we will be able to calculate the local values of the electrical conductivity, thermal conductivity and specific radiation.

Recent efforts have been concentrated on completing the experimental system, overcoming material problems, and testing the methods for data collection. A fume scrubbing system has been built to clean the sodium-potassium exhaust discharged from the test section. The scrubber (Fig. 2.-1-1) primarily consists of a series of shower-head sprinklers and filters. It eliminates the visible emission of fumes for concentrations

of sodium-potassium up to 0.5% (by weight) at an argon flow rate of 7 gms/sec.

At low cylinder pressure (a few hundred pounds per square inch) commercially available argon gas has a water content as high as 1000 p.p.m. A purification system has been constructed (Fig. 2.1-2) to eliminate the water vapor and oxygen in the argon gas. The setup consists of two chambers (in series) made of 3" diameter stainless steel tubing of 3.5 feet long. The first chamber is filled with natural manganous oxide (MnO) ore of sizes between 4 and 8 mesh. The second chamber is filled with Linde Molecular Sieve 4A, $Na_{12}\left[(AlO_2)_{12}(SiO_2)_{12}\right]\cdot 27H_2O$. The manganous oxide absorbs oxygen in the following manner

$$6\ MnO + O_2 \rightarrow 2\ MnO_3O_4$$

$$2\ Mn_3O_4 + 1/2\ O_2 \rightarrow 3\ Mn_2O_3$$

$$3\ Mn_2O_3 + 3/2\ O_2 \rightarrow 6\ MnO_2$$

$$6\ MnO + 3\ O_2 \rightarrow 6\ MnO_2$$

This reaction takes place at 150°C, and the oxygen content is reduced to less than 2 p.p.m. The molecular sieves reduce the water content in the argon gas to 1 p.p.m.

The major material difficulty encountered is to find an optically satisfactory test section as it is necessary to scan the plasma for spectrophotometic measurements. We have tested both quartz and sapphire for

window materials. Quartz becomes opaque after about 45 minutes of exposure to the plasma. This appears to be primarily due to the alkali metal vapor present. Operation at the same gas temperature with no alkali metal vapor results in no visible deterioration of the quartz. Although the chemistry of the alkali silicates seemed to indicate that the attack would be accelerated by traces of water vapor and oxygen, the installation of the gas purification system described above failed to stop the quartz deterioration.

Sapphire held up much better to the plasma but still suffered some loss of transparency. As a result of these tests, a narrow opening, i.e., an open window, was next tried. There was, of course, no difficulty with transparency. The present design of the test section is shown in (Fig. 2.1-3). Two opening gaps were provided along the test section for transverse spectrophotometric scanning. Electrodes and probes are ring-shaped to produce a uniform electric field and to obtain an average field potential measurement, respectively. The small gas leakage occuring at the gap has almost no effect on the optical and electrical measurements. An additional advantage with the provision of open gaps is the explicit prevention of shunting by the wall which can occur if a conducting film of alkali metal becomes adsorbed on the wall. The size of the gap, which is adjustable, is set at .050". This size is small enough to prevent excessive leakage and sufficiently large so that it does not become the

limiting aperture of the optical system.

A schematic diagram of the optical arrangement together with a block diagram of the associated electronic apparatus is shown in (Fig. 2.2-4). A helium discharge tube is used as a light source for testing of the instruments. The precalibrated tungsten strip lamp is provided as an absolute intensity calibration standard.

Some preliminary spectrophotometric measurements have been made the apparatus without an applied electric field. Only the sodium doublet lines 5889 Å and 5895 Å were observed. It appears that the gas temperature was simply too low in this run.

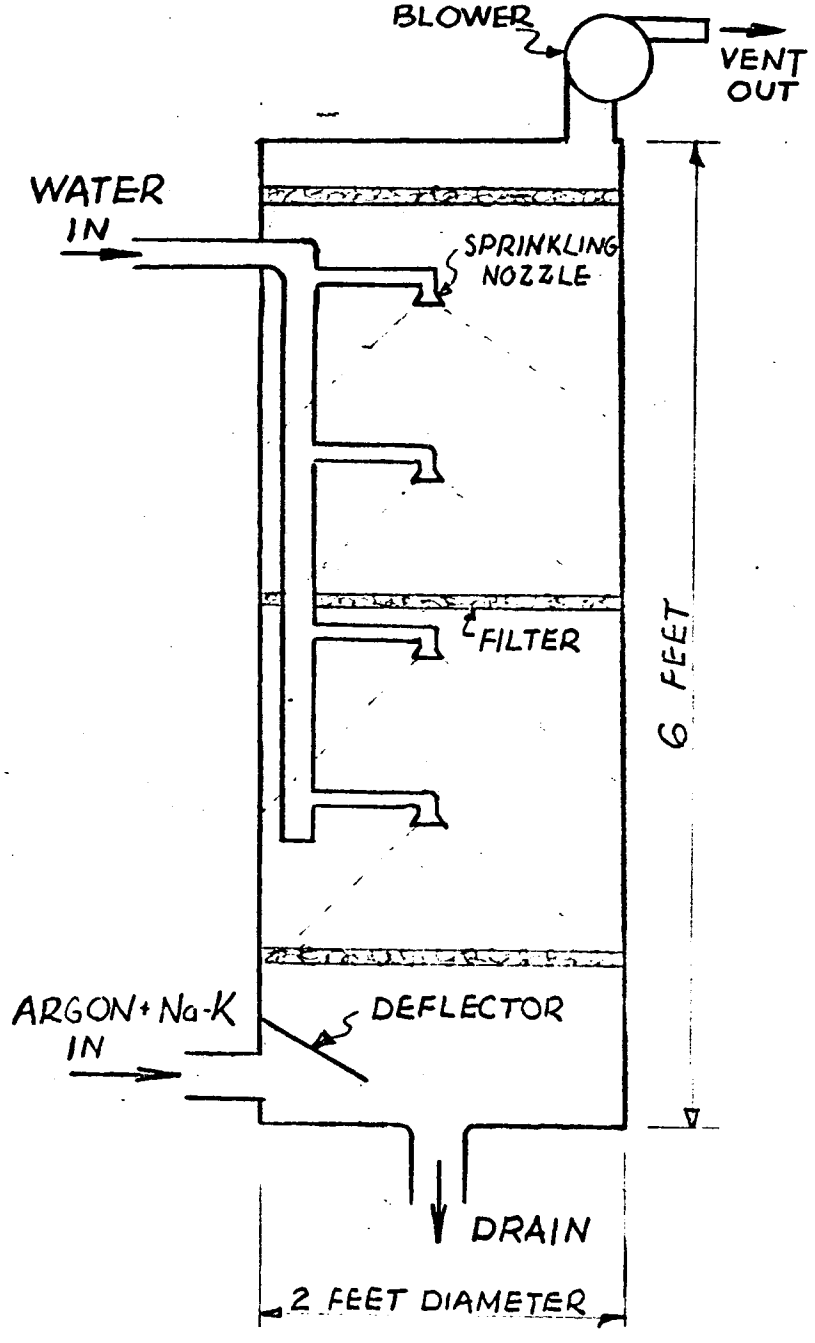

FIG. 2.1-1 Na-K FUME SCRUBBER

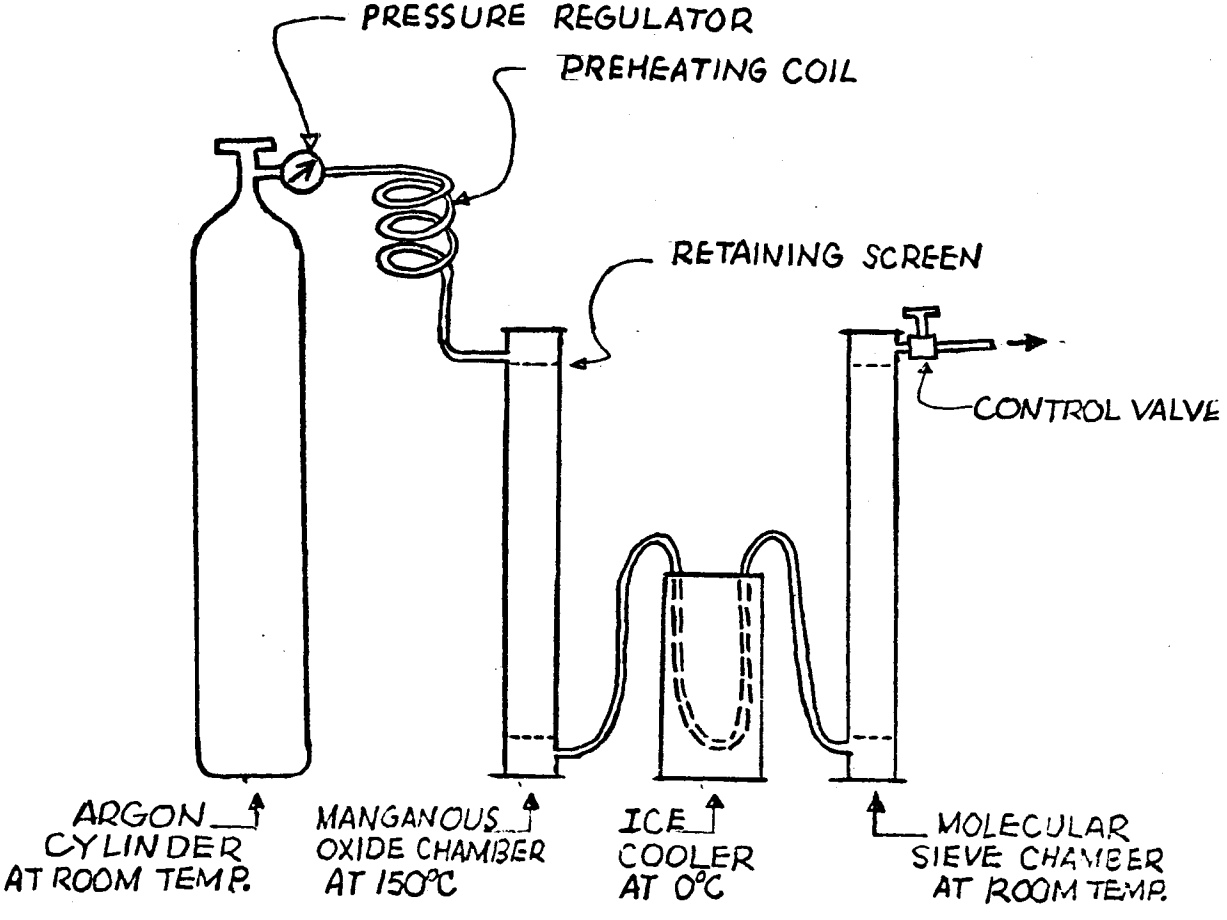

FIG. 2.1-2 ARGON GAS PURIFICATION SYSTEM

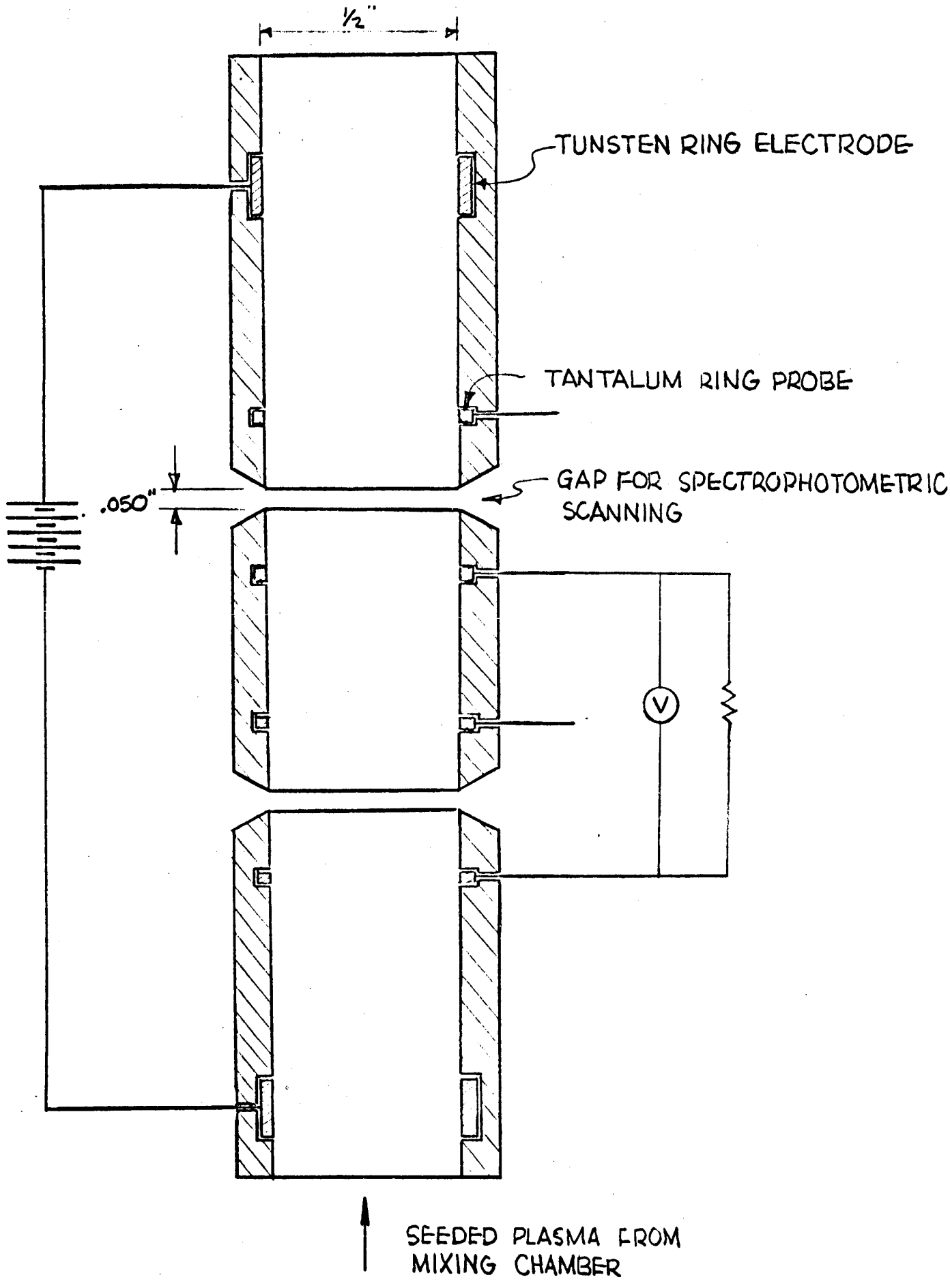

FIG. 2.1-3 TEST SECTION

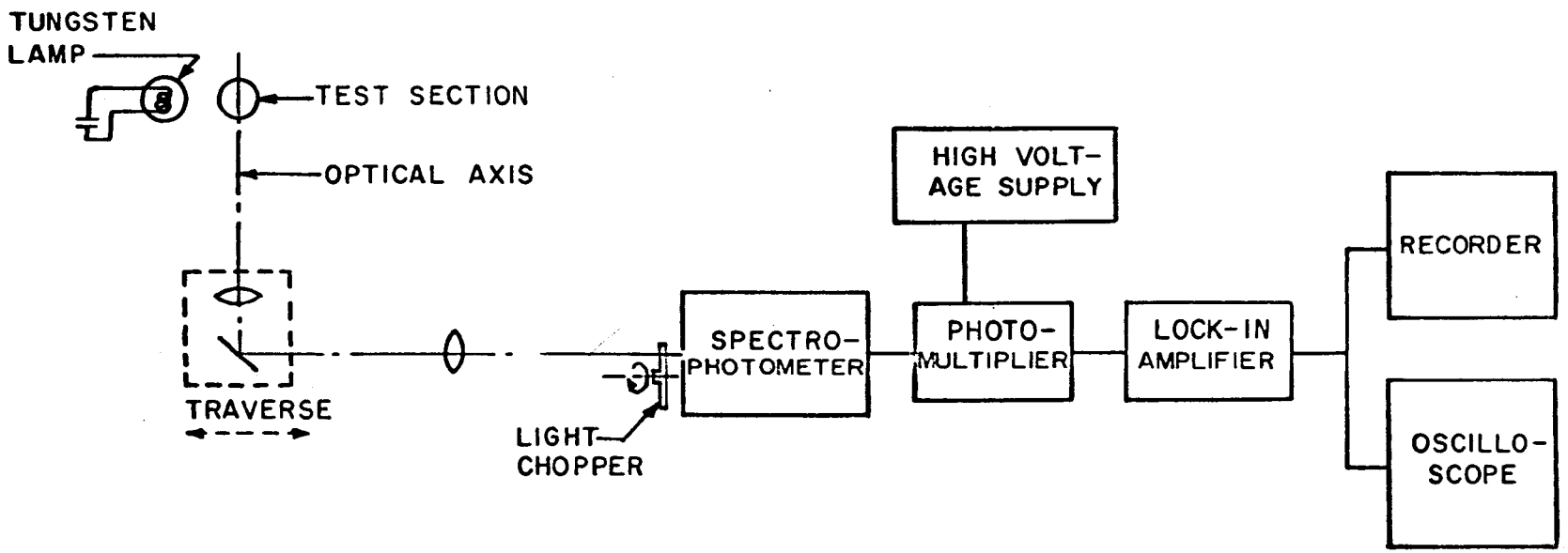

FIG. 2.1-4 INSTRUMENT BLOCK DIAGRAM

2.2 Emitter Surface Physics of Plasma Diodes

Dr. Leon W. Zelby, Dr. George L. Schrenk, M. Kaplit

The operation of close spaced (approximately 25 microns or less) passive mode thermionic energy converters depends primarily on the emitter and its interaction with the surrounding vapor (usually an electropositive element such as cesium plus some times a halogen additive). The vapor, adsorbed as a partial monolayer on the refractory metal emitter, increases the electron emission often by several orders of magnitude by lowering the emitter work function. The adsorbed particles may then be desorbed as positive ions, and these ions serve to neutralize the space charge between the emitter and the collector. There are two classes of macroscopic phenomenological models for interpreting the above characteristics of the emitter of a thermionic energy converter. In the first class are the semi-classical models; these models primarily employ the concepts of classical physics, electrostatics, thermodynamics, and statistical mechanics.[1] In the second class are those models which depend primarily on the quantum chemical concepts of ionic and covalent bonding and of electronegativity.[2] Although both classes of models can correlate emitter performance, when they are extended to untried systems, they may predict different results, such as the maximum attainable change of the emitter work function due to adsorption.

The object of this research is to obtain a microscopic understanding of the limitations of the semi-classical phenomenological model of the emitter surface of a thermionic energy converter. We are calculating quantum mechanically the microscopic charge distribution of the emitter surface, a metal-vapor interface, and are using the resulting charge distributions to determine some of the limitations of the semi-classical model of a metal-vapor interface.

The model being used for this analysis assumes that the substrate-adsorbate interaction is weak enough so that the energy distribution in the valance band of the adsorbed particles is less than k where k is Boltzmann's constant and T is the substrate temperature (see Rasor and Warner for details).[3] For a weak substrate-adsorbate interaction this metal-vapor interface can be regarded as a superposition of the surface double layer upon the electron distribution of the bulk substrate with the result that all changes in the work function due to adsorption are due to changes in the surface double layer.[4] Since we are primarily interested in predicting changes in the work function due to adsorbed partial monolayers, only the surface double layer need be studied.

At a given instant of time we are approximating the metal-vapor interface by a lattice consisting of the outermost layer of atoms of the homogeneous substrate and a homogeneous array of adsorbed particles. Depending on

the relative values of the substrate work function valence, and adsorbate ionization potential or electron affinity, there will be a transfer of charge from adsorbate to substrate or vice-versa (see Gurney for a complete discussion).[5] The remaining valence electronic charge will distribute itself in this potential well, forming the surface double layer.

Those electrons not a part of the adsorbate valence charge are assumed to be fixed symmetrically around their respective nuclei forming a so-called core. The substrate atoms are assumed to be spheres with zero valence but still capable of receiving and holding a spherically symmetric charge distribution, so that they and the adsorbate cores present point charge potentials to the fraction of valence electrons now in the interface. This procedure is a necessity since we do not know the exact charge distribution near the nucleus of these atoms in a lattice like configuration. The finite size of the cores is taken into account by assuming that the particle density is known in terms of its variational parameter for each period except in the cores where it is to be zero. For analytic convenience the cores will be represented as cubes with a volume equal to that of a sphere of radius r_m or r_f, centered at the center of the spheres and with their sides paralled to the coordinate axes.

An average of the periodic variation of the surface charge must be incorporated into the relationship between the macroscopic work function which we measure and the calculated microscopic charge density. One possible

way of doing this (which corresponds closely to the procedure used in most macroscopic studies) is to regard the electron cloud as being concentrated with respect to the transverse direction along a line through each adsorbate particle. Since each adsorbate particle occupies an identical cell, the surface double layer due only to the electron cloud is the product of the moment of a single line of concentrated charge and the number of adsorbed particles per unit area. The total surface double layer is the sum of that due to the fixed charges, represented as point charges, and the valence electron double layer. Other averages are possible but their use does not change the fundamental physics of this analysis.

This model, as described above, does not include any quantum-chemical effects nor the effects of mutual and self-depolarization of the adsorbate atoms. These effects are taken into account by varying the effective fraction of valence charge comprising the electron cloud so as to obtain the correct change in work function. In spite of these limitations and those of the approximate treatment of the cores, the final results obtained from this model are physically meaningful.

The mathematical description of the model proposed above and the quantum mechanical calculation of the surface charge distribution using the Thomas-Fermi--Dirac theory have been completed. The analytical results have been programmed for solution on an IBM 7040 computer. The details of the math-

ematical formulation and the computer program will not be presented here (see ref. &); instead we shall present a few general preliminary conclusions resulting from this analysis.

Two cases of considerable interest to thermionic energy conversion are being studied - the adsorption of a monolayer of cesium on the (100) surface of tungsten and the adsorption of half a monolayer of barium on the same clean tungsten surface. For both cases the surface charge does not extend very far out beyond the adsorbate particles, a result which is consistent with the classical concepts of adsorption. Also, we are finding that the electron-electron, and electron-nuclear interaction energies are somewhat larger than the quantum mechanical kinetic and exchange energies. These preliminary results lend some support to the semi-classical macroscopic models, such as that of Rasor and Warner.[1,3]

The proper choice of macroscopic model is extremely important to the design of thermionic energy converters - especially in the selection of emitter and collecter materials. The Levine-Gyftopoulos quantum-chemical model predicts that, for a given adsorbate, higher bare substrate work function materials have lower minimum attainable work functions.[6] The Rasor-Warner semi-classical theory, however, yields no such general rule.

This work is the first detailed macroscopic calculation of the surface

charge distribution of a metal with an adsorbed partial monolayer. It is anticipated that this work will be completed within the next several months.

References:

1. N. S. Rasor, "A Physicist's Approach to Cesiated Emitters", Thermionic Conversion Specialist Conference, Oct. 26-28, Cleveland, Ohio, 1964.
2. J. D. Levine and E. D. Gyftopoulos, "Physical Properties of Intermetallic Adsorption Systems and the Electronegativity of the Surface", Thermionic Conversion Specialist Conference, Oct. 26-28, Cleveland, Ohio, 1964.
3. N. S. Rasor and C. Warner, Jour. Appl. Phys., Vol. 35, pp 2589-2600, 1960.
4. J. R. MacDonald and C. A. Barlow, Jour. Chemical Phys., vol. 34, pp 412-422, 1963.
5. R. W. Gurney, Phys. Rev., Vol. 47, pp 479-482, 1955
6. E. P. Gyftopoulos and J. D. Levine, Jour. Appl. Phys. vol. 33, pp 67-73, 1962.
7. M. Kaplit, "The Surface Double Layer of a Metal Work Function in a Gaseous Environment", Ph.D. dissertation in preparation.

2.3 Theoretical and Experimental Investigation of a Rotating Plasma in a Crossed Electric and Magnetic Field

Dr. M. Altman, Dr. M.A. Brull, P. Hsueh

Introduction:

This is a new doctoral research problem. The basic aims and objectives of this work are summarized below. In recent years, the effects of crossed electro-magnetic fields on fluid flow have been investigated with increasing interest because of the practical needs of astronautics, plasma physics and aero-space engineering. Problems concerning the motion of a plasma in the presence of mutually perpendicular electric and magnetic fields have attracted a large amount of interest. A collection of theoretical and experimental problems have been isolated which require further work to exploit their possibilities in practical devices such as plasma accelerators, MHD power generators, and ion centrifuges. The proposed research is concerned with a plasma which is contained in a vessel bounded by coaxial cylindrical electrodes and insulated bases. A crossed field is applied to the plasma by an electric field in a radial direction, and an axial magnetic field. It is well known that the plasma will rotate around the axis of the cylinders as a result of the body force $\underline{I} \times \underline{B}$. It will start from rest and reach to an equilibrium state when the body force is compensated for by dissipation. In devices such as a rotating plasma accelerator, a vortex MHD power generator, or a rotating plasma

propulsion device, it is desirable to understand the flow phenomena so as to facilitate practical design. The following problems are proposed to be studied:

1. The analysis of the three dimensional flow phenomena taking end effect into consideration.
2. The prediction of the maximum plasma velocity with parameters which are realizable in practice.
3. The determination of energy storage properties in terms of plasma properties and the dimensions of the cylinder.
4. The heat dissipation caused by both the friction and the joule heating.
5. The stability problems of the fluid flow.
6. Experimentally verify the analytical results.

Previous Works:

A. Theoritical Part:

A. I. Gubanov and G. V. Gordeev[1] first studied the stationary case neglecting end effects. Their results included viscous effects and showed the dependence of flow velocity on magnetic flux, the radii of the electrodes, and the energy required to maintain the flow. Their calculations also showed that the maximum plasma velocity could become supersonic with parameters which were realizable in practice. ($V_{max} = 4\times10^{5}$-4×10^{6} cm/sec).

G. V. Gordeev [2] took the end effects into consideration. He considered the axial coordinate as one of the independent variables in the problem, but did not introduce seconary flow effects which should be equally important if variable z is considered. His results showed small corrections of height > outer radius; only 6% lower than the infinite length case. However, it was very much affected if height < outer radius; the maximum velocity then was only 10% of the infinite length case.

C. C. Chang and T. S. Lundgren[3] examined the possibility of using this device as a hydromagnetic capacitor. They found from their calculations that the notable feature of this device was that the maximum kinetic energy (energy stored) occurred at the moderate velocity of M = 1.5.

G. V. Gordeev[4] made the most complete analysis by considering both the transient and end effects. He solved the whole set of equations stated above by neglecting the relaxation time for establishing the applied electric field. His general results reduce to those obtained by A. I. Gubanov for the stationary case when $\frac{\partial}{\partial z} = 0$ and $t \to \infty$.

None of the papers above considered Hall currents or non-uniform $\vec{B}$ fields. E. M. Drobyshenskii[5] analized this problem by limiting the treatment to magnetic fields that were not too large, such that $\omega_i^2 \tau_i^2 << 1$ and $\omega_e^2 \tau_e^2 >> 1$. It was found that the occurance of the Hall current increases the magnetic field at the positive electrode and weakens the

field at the negative electrode. This effect was found important for values of the current strength and magnetic field intensity such that the plasma may still be regarded as stabilizd, while the conductivity is due mainly to electron mobility.

Effect of an ion wind on this problem was studied by K. V. Donskoi, E. M. Drobyshenskii and E. V. Nagarov.[6] The motion of ions in the direction of the electric field also influenced the motion of the plasma. The authors showed the possibility of expressing this force in terms of the Lorentz force over some range of the magnetic field, and "ion wind" was capable of cancelling, in some cases even overcoming, the effect of the centrifugal force.

Other American scientists like J. McCune and C. Donaldson[10] have studied this device in the reverse sense, namely as a power vortex generator.

B. Experimental Plan:

Experimental measurements were made by D. A. Baker, J. E. Hammer and F. L. Ribe[7] at the Los Alamos Scientific Laboratory. The working medium they used was a very dilute deuterium plasma at 65 ev and 1×10^{-8} g/cm^3 . In their experiment electrostatic potential and magnetic intensity were measured on the middle plan. A so-called free-wheeling operation was performed by D. A. Baker and J. E. Himmel [8] to estimate

the total energy stored in the device. No direct velocity measurement was made.

Purpose of the Proposed Research :

In the past works (1) (2) (3) (4), authors either neglected the end effects (1) (3) or considered it only partially (2) (4). In (2) (4), the authors only considered the axial coordinate as an independent variable of the rotation velocity. In other words, they considered U_θ as a function of z in addition to r. However, it is well known that when a rotating fluid is near a wall one of the essential effects is the development of an axially symmetrical boundary layer on the end walls. According to the boundary layer theory[9], the pressure gradients remain approximately constant across the boundary layer. One of the momentum equations, in this case

$$\frac{\partial P}{\partial n} = \rho \frac{U_\theta^2}{R} \quad ,$$

shows that U_θ will turn toward the center as it is closer to the boundary. A secondary flow will thus be generated. In other words, due to the presence of the end boundary, $\partial/\partial U_z$ and $\partial/\partial U_r$ will be generated. The flow will then become a three dimensional flow. According to (9) the result of an ordinary viscous flow with no field shows that U_r will decay as it is far from the wall, while U_z will remain a constant throughtout the region. Therefore, even though in (1) and (3) the authers assume a long cylinder, it should be proper only to neglect U_r and not U_z . The proposed research is aimed at providing a complete analysis of the

flow phenomena, Aside from the pure academic interest, the knowledge of U_z is valuable also in practical needs. In vortex MHD power generators, the existance of U_z is highly undesirable, for it disturbs the rotating flow and so cuts down its efficiency[10]. However, in some propulsion devices, the effect of U_z can profitably be used when the accelerated plasma is released from a nozzle installed at one end of the cylinder.

The purpose of the experimental part of this work is to verify the results obtained from the analytical part. Many assumptions and expansions made in the analysis should also be justified by actual experimental data. To avoid high temperature techniques, conducting fluids which have the same effects as the plasma in the region defined will be used as working medium. Since there has been no direct velocity measurements made before, it is proposed to measure steady state velocities in all three directions to verify the analytical results. It is also proposed to measure the magnetic field in the axial direction, since in the past works the effect of Hall currents was neglected. However, in the limit when the working medium is such that it behaves like a solid, the Hall current will not only exist but also generate an axial, spatially varying magnetic field.[11] The result will serve to verify the validity of this assumption which has widely been used by many researchers. In addition, the transition from laminar to turbulent flow will be studied.

Research Plans:

A. Analytical Part:

1. Assumptions --- Necessary assumptions will be placed on the kind of plasma we are considering such that macroscopic equations can be used, and many other microscopic effects can be neglected.

2. Basic equations and boundary conditions---If the magnetogas-dynamic approximation (assumptions stated above) is considered, then the following set of equations (in mks) express the interaction between electromagnetic and fluid dynamic effects.

MAXWELL'S EQS.

$$\nabla \times \underline{B} = \mu_o \underline{j} \qquad \nabla \cdot \underline{B} = 0$$

$$\nabla \times \underline{E} = -\frac{\partial \underline{B}}{\partial t} \qquad \nabla \cdot \underline{E} = \rho_e$$

MOMENTUM EQS.

$$\rho \frac{D\underline{V}}{Dt} = -\nabla p + \underline{j} \times \underline{B} - \rho \nabla \times (\nabla \times \underline{V})$$

$$\underline{j} = \sigma (\underline{E} + \underline{V} \times \underline{B})$$

CONTINUITY EQS.

$$\frac{D\rho}{Dt} + \nabla \cdot \underline{V} = 0$$

$$\frac{\partial \rho_e}{\partial t} + \nabla \cdot \underline{J} = 0$$

ENERGY EQ.

$$\rho \frac{Dh_o}{Dt} = \frac{\partial p}{\partial t} + \nabla \cdot (\underline{V} \cdot \underline{\underline{T}}) + \nabla \cdot (\kappa \nabla T)$$

$$+ (\nabla \times \underline{H}) \cdot [\mu_e \nu_H (\nabla \times \underline{H}) - \mu_e \underline{V} \times \underline{H}]$$

WHERE $h_o = cpt + \frac{V^2}{2}$

Boundary conditions are the conventional ones of viscous fluid flow and electromagnetic theory.

3. Possible methods of solution --- Since the above set of equations is non-linear, perturbation methods and approximate solutions will be attempted. If incompressible flow is assumed, then the momentum equations can be solved separately from the energy equation. The temperature distribution obtained from the energy equation will then serve to determine the dissipation function.

4. Desired Results:--- It is desired to obtain the following results:

(a) The velocity profile as a function of electric field, magnetic field, dimensions of the vessel and physical properties of the working medium.

(b) Amount of energy loss in order to store largest amount of energy.

(c) The stability properties.

B. Experimental Part:

The proposed experiments will include the following.

1. The construction of a test cylinder. The initial choice for the working fluid is mercury.

2. The installation of the devices that can place testing probes throughout the field.

3. Steady state velocity measurements will be made in all three directions.

4. The axial magnetic field will be measured.

C. Apparatus: Fig. 2.3-1

The major pieces of equipment needed to carry out these measurements are:

1. Testing cylinder -- As shown in Fig. 2.3-2). Since the outer shell and the axes will serve as electrodes, so the material must be close to perfect conductor to avoid potential difference along the electrodes. End plates must be insulated from the electrodes and have to be highly permeable. The dimension of the cylinder must be much greater than the dimensions of the probes such that the flow will not be disturbed.

2. A high current D.C. supply bank.

3. Magnetic field generator -- Varians Model 4004.

4. Magnetic probe diagram of the probe and the recording system.

Siemens Hall Effect Magnetic Probe is a Hall current device. Type EA218 has a dimension of 7x3.2x0.5 mm. When measuring the axial magnetic field, the typical dimension of the probe is the thickness of the device, namely, 0.5 mm. So, it is very suitable to this measurement.

5. Velocity probe -- remains to be chosen.

References

1. G. V. Gordeev and A. I. Gubanov, Tech. phy.(USSR)Vol. 3, p.1880.

2. G. V. Gordeev, Tech. Phy.(USSR) Vol. 4, p 683 (1959).

3. C. C. Chang and T. S. Lundgren, The Physics of Fluids 2 ,No.6 (1959)

4. G. V. Gordeev, Soviet Physics-Tech.Phy.,Vol.31,No.3, p 195, Sept. 1961

5. E. M. Drobyshevskii, Soviet Physics - Tech. Phy., Vol. 8, No. 11, May, 1964.

6. K. V. Donskoi, E. M. Drobyshevskii and E. V. Nazarov, Soviet Physics - Tech. Phy., Vol. 8, No. 11, May 1964.

7. D. A. Baker, J. E. Hammel, and F. L. Ribe, The Physics of Fluids, Vol. 4, No. 12, Dec. 1961.

8. D. A. Baker and J. E. Hammel, The Physics of Fluids, Vol. 4, No. 12, Dec., 1961.

9. H. Schlichting, "Boundary Layer Theory".

10. NASA Report Contract No. NAS 3-2526 "Research on the Vortex MDH power generator".

11. K. Boyer, J. E. Hammel, C. L. Longmire, D. Nagle, F. L. Ribe and W. B. Riensenfeld. "Proceedings of the Second United Nations International Conference on the Peaceful Uses of Atomic Energy, held in Geneva, Sept., 1958. Vol. 31, "Theoritical and Experimental Aspects of Controlled Nuclear Fusion".

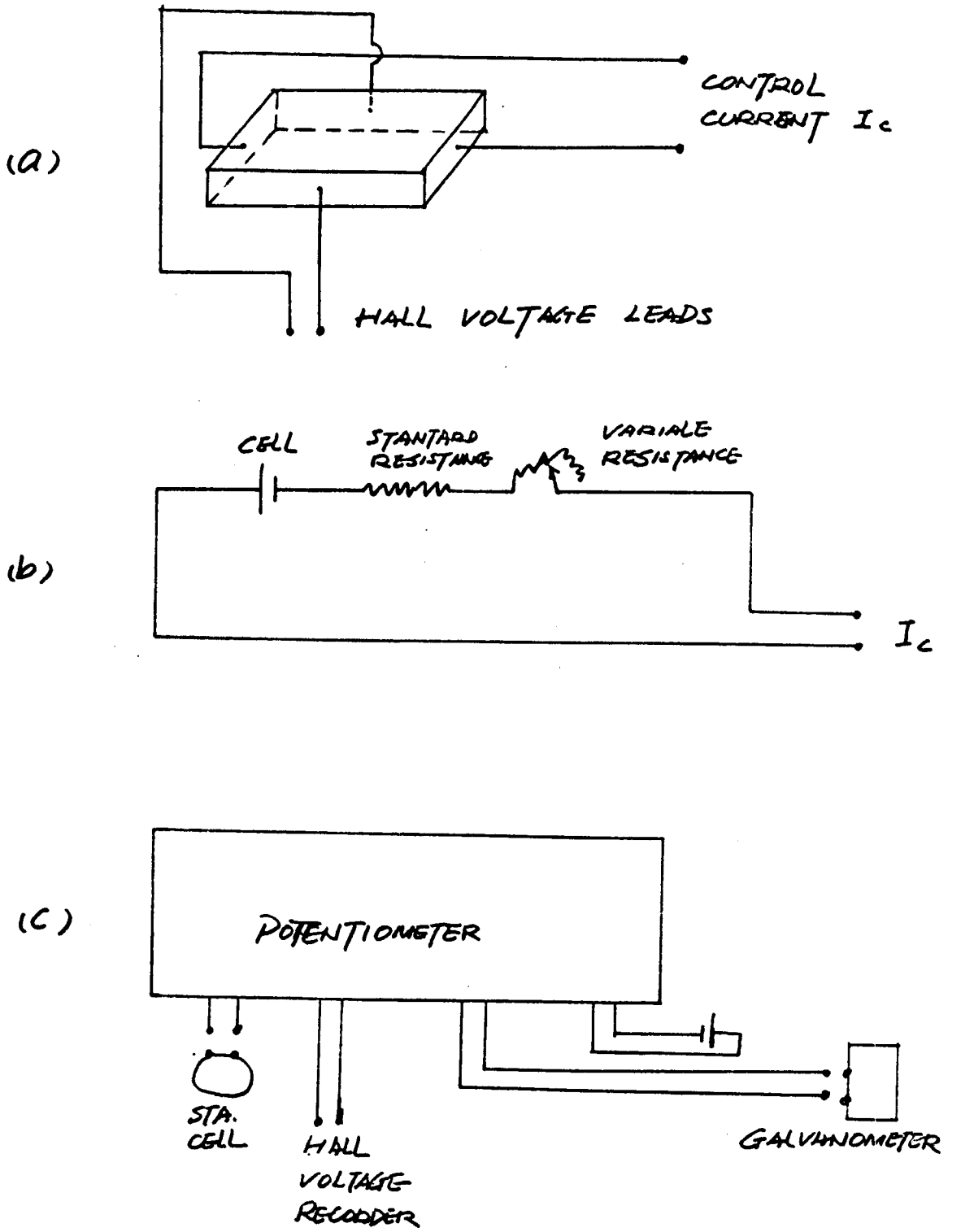

Figure 2.3-1. (a) Hall effect magnetic probe. (b) Control current circuit (c) Hall voltage circuit.

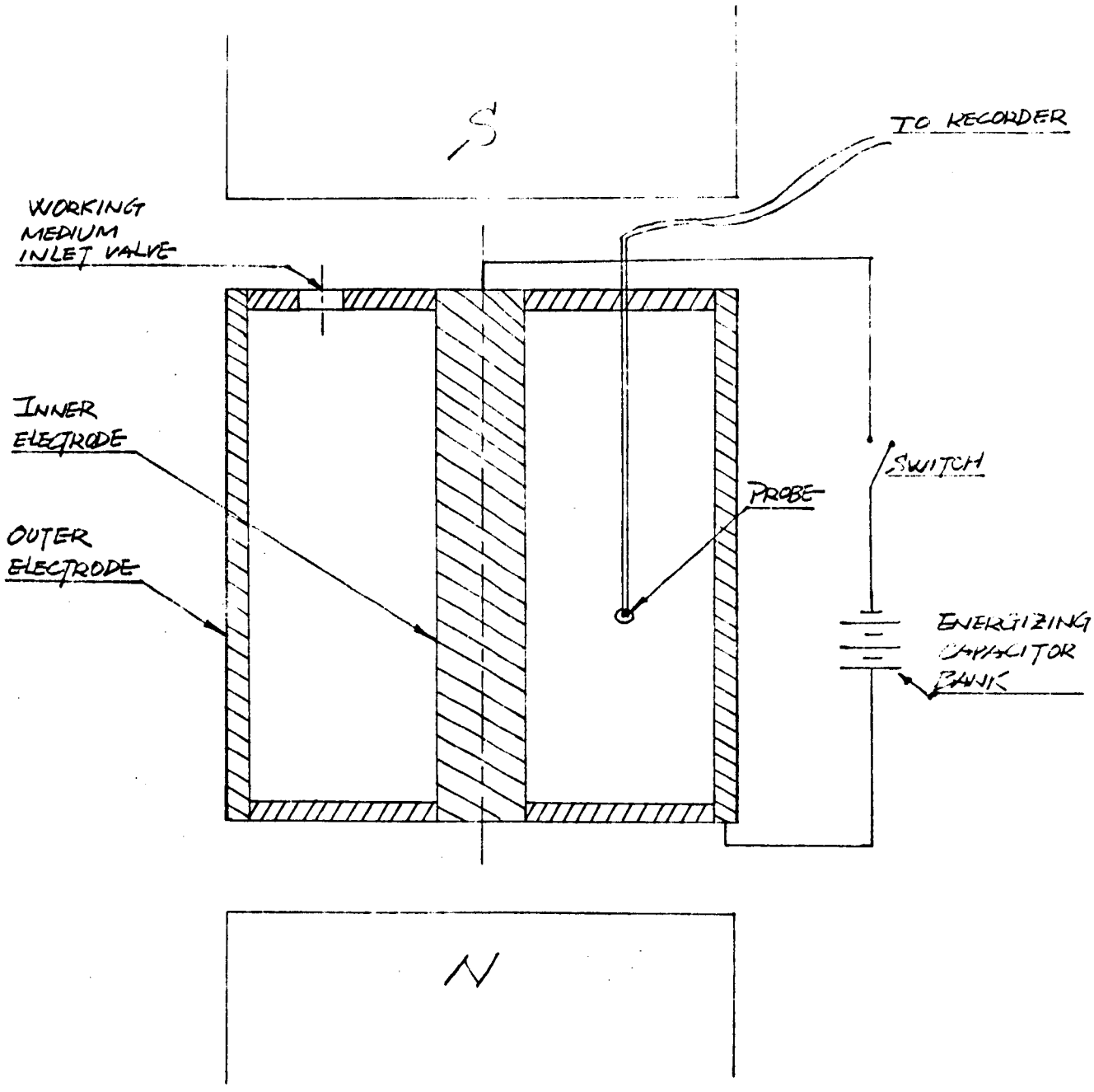

Figure 2.3-2 Schematic diagram of the testing cylinder

3. ELECTROCHEMICAL ENGINEERING

Branch Chief: Dr. Leonard Nanis

3.1 Transient Concentration Polarization in Natural Convection Electrolysis

Dr. Leonard Nanis and Akin Adubifa

In a previous report [1], the time variation of the concentration changes at electrodes was considered for constant current passage. It was shown that two mathematically soluble hypothetical cases bounded the actual performance and a means was suggested for evaluating the thickness of the finally established boundary layer. The various diffusion problems treated were in terms of concentrations and it remains to correlate the theoretical findings with the observable phenomenon, namely the time variation of concentration overvoltage.

In order to consider the actual variation of concentration overvoltage with time, the fraction of ultimately attained concentration difference at x = o may be expressed in terms of the steady state overvoltage with the aid of the Nernst Equation. By defining overvoltage with respect to the potential of a similar electrode in the same electrolyte in the absence of current passage, for the anode there is obtained

$$\frac{\left[C_{o,\tau} - C_b\right]}{\left[C_{o,\infty} - C_b\right]} = \frac{\left[e^{z\eta F/RT} - 1\right]}{\left[e^{z\eta_\infty F/RT} - 1\right]} \qquad (1)$$

where η = polarization at time τ

η_∞ = ultimately attained polarization ($\tau = \infty$)

R = gas constant

T = absolute temperature

By taking the absolute value of cathodic polarization, there is similarly obtained

$$\frac{[C_{o,\tau} - C_b]}{[C_{o,\infty} - C_b]} = \frac{[C_b - C_{o,\tau}]}{[C_b - C_{o,\infty}]} = \frac{1 - e^{-z\eta F/RT}}{1 - e^{-z\eta_\infty F/RT}} \qquad (2)$$

Both Eq. 1 and 2 may be approximated for the condition by expansion of the exponential terms with retention of first order arguments only. This leads to

$$\frac{[C_{o,\tau} - C_b]}{[C_{o,\infty} - C_b]} = \frac{\eta}{\eta_\infty} \qquad (3)$$

which is a truly linear function at room temperature only if the ultimately attained overvoltage is very small, i.e.

Eq. 3 should be more useful for higher temperature systems, e.g., molten salt electrolytes. For computation concerning agueous systems, a tabulation of the general term in both Eq. 1 and 2 has been given in Appendix 1 for 25°C and may be used for temperatures within $\pm$ 5 degrees. Sample calculations are shown in Fig. 3.1-1 for the variation of anode

and cathode overvoltage with time following the start of constant current passage, based upon chosen values of η_∞ = 10 mV, z = 2, $D = 5 \times 10^{-6} cm^2 sec^{-1}$ and δ = 0.01 cm. It should be remembered that the fictitious δ based on a linear gradient is used as the basis of the computation and that the real boundary layer thickness is twice this value or 0.02 cm in the present case. Eq. 4.1-6 and 4. 1-8 of reference 1 (Curves 1 and 2 of Fig. 3.1-2, Ref. 1) have been followed. By referring to Fig. 3.1-2 of Ref. 1, the actual variation of concentration at the electrode may be expected to follow the dotted line of Fig. 3.2-1 beyond the point of separation of the pre-existing δ and pure diffusion hypothetical cases. Beyond the point of separation (about 5 seconds), the actual time trace should bend away from the dotted line and at about 15 seconds should cross the solid line and remain below this solid line. For the anode in particular, it may be appreciated that there would be considerable difficulty in distinguishing between the various cases at longer times. For the cathode, this distinction could be more apparent. For the anode, about 7 mV are attained before the theoretical separation time (τ = 0.333), which for both anode and cathode is discernible only after six seconds (real time) of current passage.

In practice, the actually observed η vs τ variation generally includes a vertical rise at t = o because of the resistive potentials due to the electrical field between the vertical electrode and the tip of a probe

reference electrode. Also, the present analysis is really valid for the absence of other forms of overvoltage. If, however, activation overvoltage is a rapidly rising function of time, both it and the resistive drop will appear as a vertical rise at $t = 0$ for the time scale shown in Fig. 3.1-1. Strictly, the time variation of the resistive drop due to changing electrolyte concentration has also to be treated. Analysis of concentration-overvoltage vs time curves may be used to evaluate the actual thickness of the boundary layer formed in electrolyses governed by natural convection. Times for attainment of a given fraction of ultimate η_∞ should be strongly dependent on the actual magnitude of δ since τ contains the inverse square of δ. Fig. 3.1-2 shows the expected $\eta - \tau$ curves for three δ values differing by only 0.001 cm in extent for times up to the analytical separation point at $\tau = 0.333$. Real boundary layer thickness values actually would differ by 0.002 cm. For the anode, it may be seen that for an attainment of 6.5 mV out of 10 mV, the curves for the different δ values are each separated by a time of one second. Such time resolution is readily attainable experimentally by means of an oscilloscope or chart oscillograph. Analysis of actual traces requires knowledge of η_∞, so that in practice, the resistive and other rapidly rising overvoltages must be subtracted from the steady state potential and accordingly from the observed η values over the time span. Several plotting methods of the

vs. t data may be used to extract the value of δ.

For example for the cathode, Eqn. 2 and Eqn. 4. 1-6 of Ref. 1 may be arranged as

$$1 - e^{-z\eta F/RT} = \left[1 - e^{z\eta_\infty F/RT}\right] \frac{2}{\pi^{1/2}} \frac{D^{1/2}}{\delta} t^{1/2} \qquad (4)$$

Knowledge of η_∞ and D combined with the square root of time plot suggested by Eqn. 4 can permit the evaluation of δ.

Work is presently in progress to check the above conclusions using vertical silver anodes dissolving into various concentrations of silver nitrate. This electrode-electrolyte system was chosen because of the very large exchange current density, thus avoiding problems associated with the existence of activation overvoltage. Primary variables will be the vertical position on the electrode and the current density. Values for the diffusion coefficient will be taken from the recent work of Firth and Tyrell.[2] Literature values for the density and viscosity of silver nitrate solutions will be used for the calculation of the expected boundary layer thickness as theoretically evaluated by Ibl.[3]

A program has been written for machine computation of tables of the general term in Equations 1 and 2 in order to speed the analysis of the overvoltage vs time traces for δ evaluation. A sample of the tables,

rounded to four significant figures, is given in Appendix 1.

References:

1. INDEC-SR-5, Section 4.

2. J. G. Firth and H. J. V. Tyrell, Journal of the Chemical Society, p 2044, May - Aug. 1962.

3. Ibl, N., Advances in Electrochemistry & Electro-chemical Eng., Vol. 2, p 86, Intersciences 1962.

APPENDIX 1

$z\eta$, mV	CATHODE $1 - e^{-z\eta F/RT}$	ANODE $e^{-z\eta F/RT} - 1$
0	.0000	.0000
1	.0380	.0396
2	.0746	.0807
3	.1099	.1234
4	.1437	.1679
5	.1763	.2141
6	.2078	.2621
7	.2378	.3120
8	.2668	.3639
9	.2947	.4179
10	.3216	.4739
11	.3474	.5322
12	.3722	.5929
13	.3961	.6559
14	.4191	.7214
15	.4412	.7895
16	.4624	.8602
17	.4829	.9338
18	.5026	1.0103
19	.5215	1.0898
20	.5397	1.1725
21	.5572	1.2585
22	.5741	1.3478
23	.5903	1.4406
24	.6059	1.5372
25	.6209	1.6376

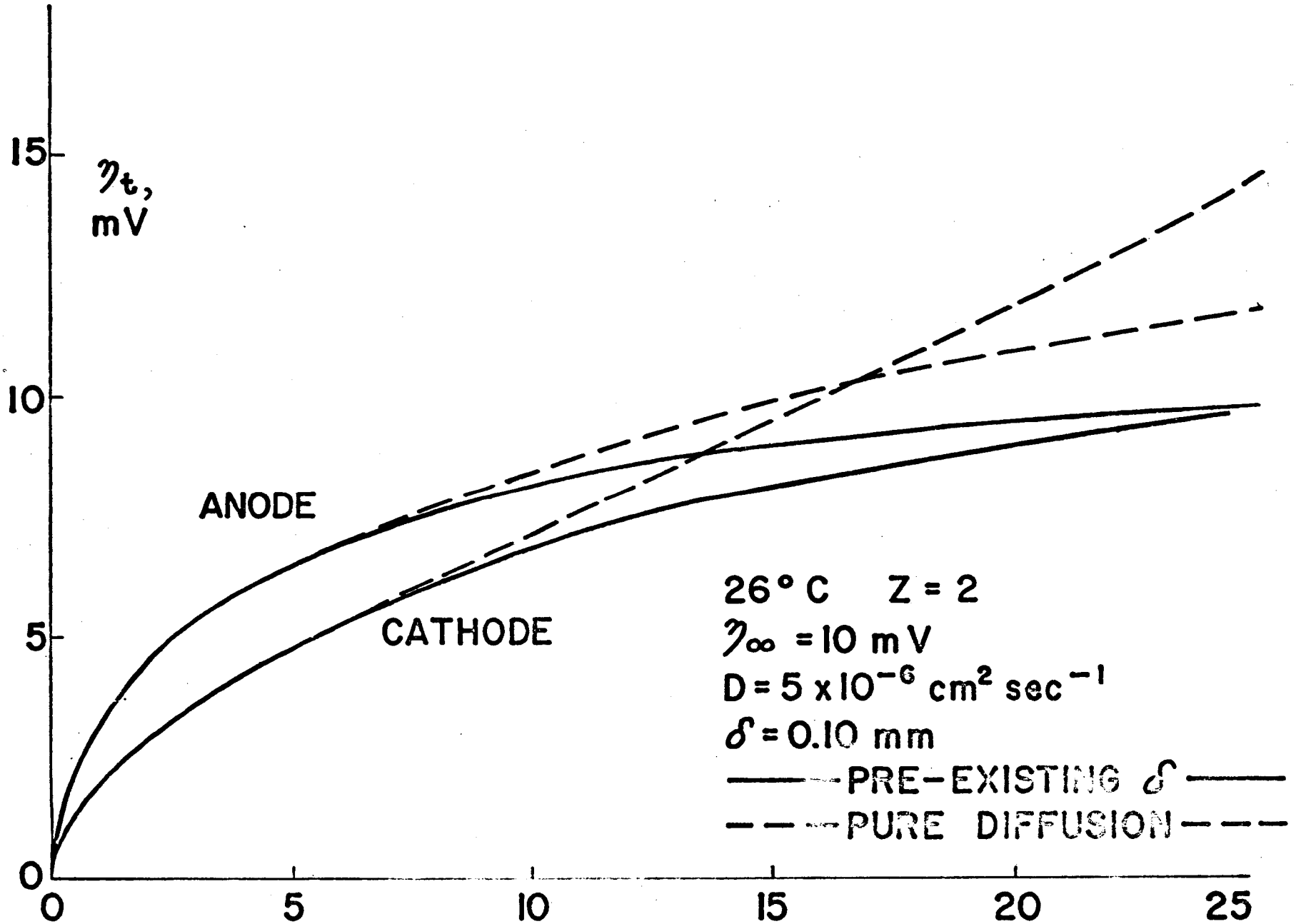
15
10
5
0
η_t, mV
ANODE
CATHODE
26° C Z = 2
η_∞ = 10 mV
D = 5 x 10^{-6} cm^2 sec^{-1}
δ = 0.10 mm
PRE-EXISTING δ
PURE DIFFUSION
0
5
10
15
20
25
TIME, sec

FIG. 3.1-1